AFRL-AFOSR-JP-TR-2018-0069

Ultrastrong Carbon Thin Films from Diamond to Graphene under Extreme Conditions: Probing Atomic-Scale Interfacial Mechanisms to Achieve Ultralow Friction and Wear

Robert Carpick
TRUSTEES OF THE UNIVERSITY OF PENNSYLVANIA
3451 WALNUT ST
PHILADELPHIA, PA 19107-6205

09/20/2018
Final Report

Air Force Research Laboratory
Air Force Office of Scientific Research

Asian Office of Aerospace Research and Development
Unit 45002, APO AP 96338-5002

REPORT DOCUMENTATION PAGE

Form Approved
OMB No. 0704-0188

1. REPORT DATE *(DD-MM-YYYY)* 20-09-2018	**2. REPORT TYPE** Final	**3. DATES COVERED** *(From - To)* 28 Sep 2015 to 27 May 2018

4. TITLE AND SUBTITLE Ultrastrong Carbon Thin Films from Diamond to Graphene under Extreme Conditions: Probing Atomic-Scale Interfacial Mechanisms to Achieve Ultralow Friction and Wear	**5a. CONTRACT NUMBER**
	5b. GRANT NUMBER FA2386-15-1-4109
	5c. PROGRAM ELEMENT NUMBER 61102F
6. AUTHOR(S) Robert Carpick	**5d. PROJECT NUMBER**
	5e. TASK NUMBER
	5f. WORK UNIT NUMBER
7. PERFORMING ORGANIZATION NAME(S) AND ADDRESS(ES) TRUSTEES OF THE UNIVERSITY OF PENNSYLVANIA 3451 WALNUT ST PHILADELPHIA, PA 19107-6205 US	**8. PERFORMING ORGANIZATION REPORT NUMBER**
9. SPONSORING/MONITORING AGENCY NAME(S) AND ADDRESS(ES) AOARD UNIT 45002 APO AP 96338-5002	**10. SPONSOR/MONITOR'S ACRONYM(S)** AFRL/AFOSR IOA
	11. SPONSOR/MONITOR'S REPORT NUMBER(S) AFRL-AFOSR-JP-TR-2018-0069

12. DISTRIBUTION/AVAILABILITY STATEMENT
A DISTRIBUTION UNLIMITED: PB Public Release

13. SUPPLEMENTARY NOTES

14. ABSTRACT

The goal was to gain a fundamental understanding of how to achieve low friction and wear in ultrastrong carbon-based materials. Experimentally, in situ nanotribometry method was used to enable nanoscale visualization of sliding contacts inside the TEM. These experiments are in turn modelled computationally using molecular dynamics, allowing better understanding of the atomic scale processes controlling friction and wear. The focus was on the behavior of silicon-silicon, silicon-diamond, and diamond-like-carbon (DLC)-diamond interfaces. For silicon-silicon interfaces, the nanocontacts showed a sliding-history and stress-dependent (applied normal stress) adhesion; sliding increased adhesion by more than 16 times. This is explained in terms of stress-activated covalent bond breaking that only occurs during sliding. For silicon in sliding contact with diamond, adhesion increased with applied stress and speed. This dependence is explained in terms of tip geometry changes due to atomic-scale plasticity. For DLC, wear during sliding and the evolution of adhesion forces were characterized. Wear was measured as a function of load and sliding distance. Gradual wear with sliding was observed with the wear rate increasing with the average contact stress. It neither followed the classic Archards wear law nor recently observed behavior following transition state theory. The wear behavior over the full range of stresses is well described by multi-bond wear model that exhibits a change from Archard-like behavior at high stresses to a transition state theory description at lower stresses. Adhesion showed large scatter, which was attributed to stochastic covalent bond breaking and formation events. In summary, this work shows that understanding adhesion and wear requires careful consideration of the interplay of mechanics and chemistry at the interface.

15. SUBJECT TERMS
Tribology, Surfaces, Graphene, Diamond, Single Asperity, Modeling

16. SECURITY CLASSIFICATION OF:			**17. LIMITATION OF ABSTRACT**	**18. NUMBER OF PAGES**	**19a. NAME OF RESPONSIBLE PERSON** WINDER, SHEENA
a. REPORT	**b. ABSTRACT**	**c. THIS PAGE**			
Unclassified	Unclassified	Unclassified	SAR		**19b. TELEPHONE NUMBER** *(Include area code)* +81-42-511-2008

Standard Form 298 (Rev. 8/98)
Prescribed by ANSI Std. Z39.18

Final Report for AOARD Grant # FA2386-15-1-4109

"Ultrastrong Carbon Thin Films from Diamond to Graphene under Extreme Conditions: Probing Atomic-Scale Interfacial Mechanisms to Achieve Ultralow Friction and Wear"

Aug. 26, 2018

PI and Co-PI information:

U.S. Awardee
Robert W. Carpick
Email: carpick@seas.upenn.edu
University of Pennsylvania (Penn)
Mechanical Engineering and Applied Mechanics
229 Towne, 220 S. 33rd St., Philadelphia, PA, 19104-6315, USA
Tel: 215-898-4608
Fax: 215-573-6334

Asia (Taiwan) Awardee
Yeau-Ren Jeng
E-mail: imeyrj@ccu.edu.tw
National Chung Cheng University (CCU)
Department of Mechanical Engineering,
Ming-Hsiung, Chia-Yi 621, Taiwan
Tel: 886-5-2428189
Fax: 886-5-2720589

Period of Performance: 05/28/2017– 05/27/2018

Abstract: Our goal was to gain a fundamental understanding of how to achieve low friction and wear in ultrastrong carbon-based materials. Experimentally, we used an *in situ* nanotribometry method, which enables nanoscale visualization of sliding contacts inside the transmission electron microscope (TEM). These experiments are in turn modelled computationally using molecular dynamics, allowing better understanding of the atomic-scale processes controlling friction and wear. Since the last report, we focused on the behavior of silicon-silicon, silicon-diamond, and diamond-like-carbon (DLC)-diamond interfaces. For silicon-silicon interfaces, we found that nanocontacts showed a sliding-history and stress-dependent adhesion, where sliding increased adhesion by more than 16 times, and this effect was enhanced by the applied normal stress. We explain this in terms of stress-activated covalent bond breaking that only occurs during sliding. For silicon in sliding contact with diamond, we observe that the observed adhesion increases with applied stress and speed, and explain this dependence in terms of tip geometry changes due to atomic-scale plasticity. For DLC, we characterized wear during sliding, and the evolution of adhesion forces. Wear was measured as a function of load and sliding distance. Gradual wear with sliding was observed with the wear rate increasing with the average contact stress, but not following the classic Archard's wear law nor to recently observed behavior following transition state theory. The wear behavior over the full range of stresses is well described by multi-bond wear model that exhibits a change from Archard-like behavior at high stresses to a transition state theory description at lower stresses. We then observed that adhesion showed large scatter, which we attribute to stochastic covalent bond breaking and formation events. In summary, this work shows that understanding adhesion and wear requires careful consideration of the interplay of mechanics and chemistry at the interface.

1 Introduction

Our goal is to characterize and understand the atomic-scale mechanisms governing the tribological behavior (friction and wear) of hard carbon materials during initial sliding contact, in order to understand what controls and enables the transition from high to low friction and wear. Developing this scientific insight is important to enable widespread usage of these materials to applications such as vibrating joints[1,2], contacting and sliding surfaces in micro- and nanoelectromechanical systems for sensors and actuators[3], joints in vacuum or anhydrous environments (as found in the **upper atmosphere and in outer space),** and protective coatings for bearings, bushings, and gears in engines[4,5], turbines[6,7], and other aerospace components. The research was carried out using a unique *in situ* transmission electron microscopy (TEM) nanotribometry method that both PI's have collaboratively developed, thanks in part to prior AOARD support. This method allows us to visualize and quantify atomic-level processes occurring in sliding contacts through real time, real space, high resolution TEM measurements of a contact pair, where contact forces are precisely measured and controlled.

1.1 Current Challenges in Tribology of Carbon-Based Materials

The mechanical and tribological properties of carbon-based films are, under the right conditions, superior to almost all other materials. Diamond, the stiffest and hardest bulk material known, can be grown in a smooth nanocrystalline thin film form with equivalent mechanical performance (ultrananocrystalline diamond - UNCD). These films can exhibit friction coefficients of 0.01 and less (as slippery as ice), and wear rates corresponding to fractions of an atomic layer per pass of the sliding interface ($<10^{-10}$ $mm^3N^{-1}m^{-1}$) with no lubricant needed [8-10]. These characteristics far exceed those of well-lubricated interfaces of high performance steels and other expensive coatings.

Despite this potential, the widespread use of these materials is inhibited by a lack of scientific understanding of the initial process of wear, the so-called “run-in” process. While the steady-state wear rate and friction is often low, the *initial* rate of friction and wear during the “run-in” period, can be high. This “run-in” period may consist of only a few cycles of sliding, during which the contacting asperities become smoother, and local stresses, friction, and wear decrease, sometimes by *orders of magnitude*. However, in some cases, this “run-in” continues indefinitely [11-14]. This is a catastrophic outcome: sliding parts can wear out far earlier than expected, or seize. Small changes in load, environment, sliding rate, surface roughness, and sample preparation have been observed to affect whether or not this crucial transition takes place. Results are largely empirical; there is a lack of scientific understanding of the atomic-scale processes in the contact that control whether the transition to low friction and wear occurs. Developing fundamental knowledge of these processes is crucial, and is the key to rationally designing and controlling coatings and operating parameters so that stable, low, reliable friction and wear performance can be obtained for engineered systems using these materials.

Previous studies by the PIs on interfacial contact conditions including atomic and macro scale studies show that the behavior of individual asperity contacts at the nanoscale plays a critical role in the run-in process[15-19]. More recent research, including by the both PI’s, points toward specific atomic-scale mechanisms strongly affecting the sliding behavior of these materials, including: rehybridization from sp^3 to sp^2-bonding of the C atoms[20], formation of bonds across the interface and subsequent atomic bond breaking[21], and the strong passivating influence of small quantities of adsorbates[9,22]. However, many of these observations are indirect or inferred, and others have not been studied in a systematic way that allows understanding of the run-in transition (namely the contact interactions on the surface separation and the real contact area for an asperity) to be investigated.

2 Experimental methodology

2.1 *In situ* TEM Tribometry

To address our research goals, over the last few years we have developed a unique *in situ* TEM tribometry method that allows atomic-scale characterization of a single-asperity sliding contact. Both PI’s Carpick and Jeng have a Hysitron PI-95 PicoIndenter TEM specimen holder, which was used for this purpose. This instrument measures normal load and displacement simultaneously inside a TEM, and can position an indenter in three dimensions with nanometer scale precision (Figure 1). While the standard configuration is designed for indentation, we developed a method for laterally sliding the indenter (by using integrated piezoelectric controls) against an atomic force microscope (AFM) cantilever. In this configuration, we can study the sliding behavior of several contact pairs (one material in the indenter, other material in the AFM tip) while observing the process with the TEM, allowing atomic-scale resolution of the mechanisms of deformation, adhesion, friction, wear, and failure at the sliding interface.

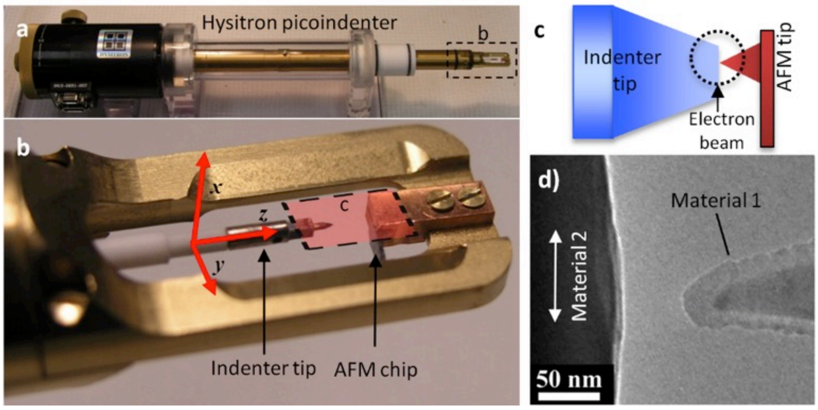

Figure 1: *In situ* TEM setup. (a) The Picoindenter TEM holder. The dashed rectangle is shown in b) in more detail. A piezo tube allows the indenter to attain three dimensional motion with sub-nm resolution. (c) Schematic close up of the AFM cantilever and indenter tip. (d) TEM micrograph of a typical experiment, where characterization of the sliding contact between the material of the AFM tip (#1) and the material of the indenter (#2) can be visualized with high resolution

The *in situ* TEM methodology has the key advantages of live-imaging the process of wear and of resolving volumes removed from the sliding asperity as low as 25 nm^3 in volume[23]. These capabilities are critical for probing the run-in period of wear. Moreover, since the measurements are carried out *in situ*, the analytical and crystal-characterization capabilities of the TEM can be leveraged to obtain further insights on the wear processes. All these can be done in sequence with sliding experiments to observe and understand the structural changes occurring.

As part of the present project, the PI developed and published a method for enabling characterization of AFM cantilever probes in the AFM[24]. While scanning probe microscopy (SPM) enables detailed characterization of the geometric, mechanical, and transport properties of surfaces, the technique is often hindered by incomplete knowledge of the shape of the scanning probe. Various authors have measured tip geometry using scanning of known features or imaging of the tip using electron microscopy. The former technique requires complex numerical algorithms with multiple analysis parameters; the latter typically requires custom fixturing and suffers concerns about repeatability and contamination. Here we demonstrate a novel fixture and a practical guide to imaging SPM probes using electron microscopy, which minimizes or eliminates these disadvantages. The dissemination of this fixture and technique will enable a broader community of researchers to improve the quality of SPM imaging and the quantitative analysis of results.

The experimental procedure consists of bringing the indenter surface and AFM tip in contact; the force is controlled by displacing the indenter beyond this point a given amount against the AFM tip, whose spring constant has been calibrated before. Subsequently, lateral sliding motion at a predetermined speed and duration is imposed on the contact. After sliding is finished, the contact is separated. This process is captured on video, allowing post-processing analysis for metrology of the force and observation of failure events. Furthermore, before and after sliding, high-resolution images of the tip are recorded, thus allowing visualization of volume loss (wear) due to sliding (quantified in post-processing), and of any structural change.

2.2 *In situ* TEM Nanoindentation Experimental methodology: tip on tip and tip on flat

The experimental methodology using the followed here is identical to the methodology in Ref. [1] except where an AFM tip was used as the lower surface in place of a diamond indenter. The following gives a detailed account of the methodology.

The upper AFM cantilever spring constants in these experiments were calibrated with the Sader method[2]. The spring constants ranged from 0.20 to 1.51 N/m. The experimental steps were:

1) obtain images of the upper AFM probe at a range of magnifications; magnifications from 40kx to 80kx are optimal for subsequent comparison to tip images after sliding since they include features from the sides of the tips (the shank), which provide stable fiducial markers to align images before and after each sliding test,

2) align the upper silicon probe in the focal plane of the lower diamond indenter or silicon probe,

3) slowly (<1 nm/s) bring the lower probe or indenter toward the upper silicon probe using fine z-positioning whereupon a snap-in of the cantilever and probe occurs when the gradient of the probe-sample interaction force (primarily due to van der Waals (vdW) attraction) exceeds the spring constant of the cantilever,

4) execute sliding if desired,

5) halt sliding and slowly (<13 nm/s) manually retract the diamond indenter or lower silicon probe to break contact; adhesion will keep the upper probe in contact with the indenter or lower probe until the spring force from the upper cantilever exceeds the adhesive force, at which point the upper probe quickly snaps off of the indenter's surface, and

6) obtain images of the upper probe at similar or identical magnifications and conditions as the pre-test images from step 1.

3 Results and Discussion

3.1 Silicon adhesion probed with the *in situ* TEM nanoindentation methodology

Silicon is the most abundant element in terrestrial rock, it is the primary material used in the semiconductor industry, and is the primary material used in scanning-probe microscopy (SPM or AFM) and tip-based nanolithography (TBN) research and industries. Thus, a complete understanding of its surface properties and interactions with other materials of interest is of general importance. Using our unique *in situ* TEM nanoindentation and sliding methodology, we discovered never before observed adhesion phenomena experienced by self-mated silicon contacts and silicon against diamond. Though adhesion generally increases with sliding speed and stress regardless of the material pair, there are clear differences between them in the mechanisms controlling adhesion.

3.1.1 Self-mated silicon nanoasperities show sliding-history and stress-dependent adhesion

Six groups *in situ* TEM tip-on-tip nanoindentation and sliding experiments were done on six different days with different self-mated silicon probe systems. The native silicon dioxide was removed by either wearing it off prior to recording data or by fracturing the apexes of each probe before acquiring data. Figure 2 provides details for the history of each probe system. Tests done within a group were either contact-separate (CS) or contact-slide-separate (CSS). As their names indicate, CS tests had no sliding whereas sliding was induced after coming into contact during CSS experiments.

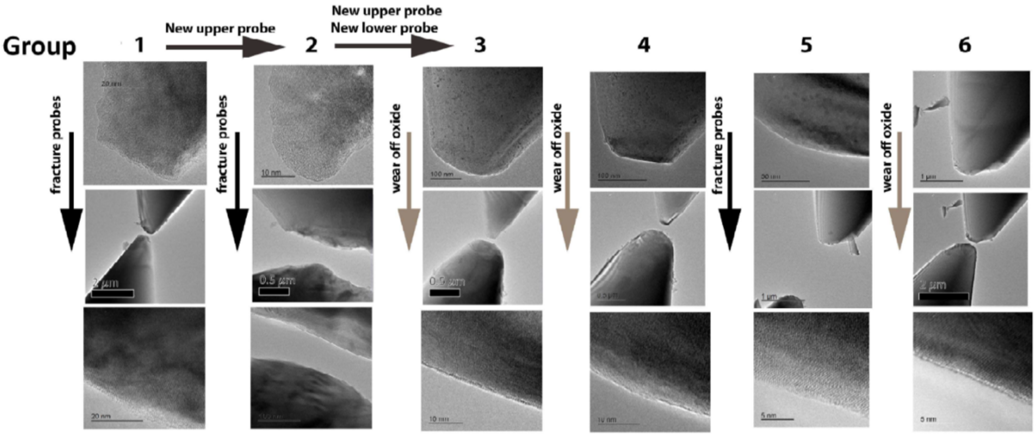

Figure 2 Images of the probes used in the six groups of experiments (columns labeled by experiment number) taken before all experiments in that group (first row), during a representative experiment in that group (middle row), and after a representative experiment in that group (bottom row). Down arrows indicate whether the oxide was removed via wear or fracture and right arrows indicate when a different probe from the previous probe was used.

Over two hours of video consisting of 433 CS and CSS experiments was captured and is available at this link https://youtu.be/CE1ROm_rmXg

The videos clearly show that adhesion is very low when performing a CS experiment, but it surprisingly increases substantially when sliding is induced during a CSS experiment. Furthermore, when a CS experiment is performed immediately following a CSS experiment the adhesion usually returns to low or undetectable values. This is the first observation of reversible i.e., sliding-history-dependent adhesion for any material and certainly the first observed *in situ*. This phenomenon has important implications for tunable adhesion technologies like transfer printing and pick-an-place manufacturing where the ability to control the magnitude of adhesion is critical.

Statistics of the adhesion force are shown in Figure 3 and are differentiated by group, demonstrating the significant statistical increase of adhesion that occurs when sliding is induced. Overall, there was an average of 19 times increase in adhesion from CSS tests over CS tests and increases as high as 32 times were measured.

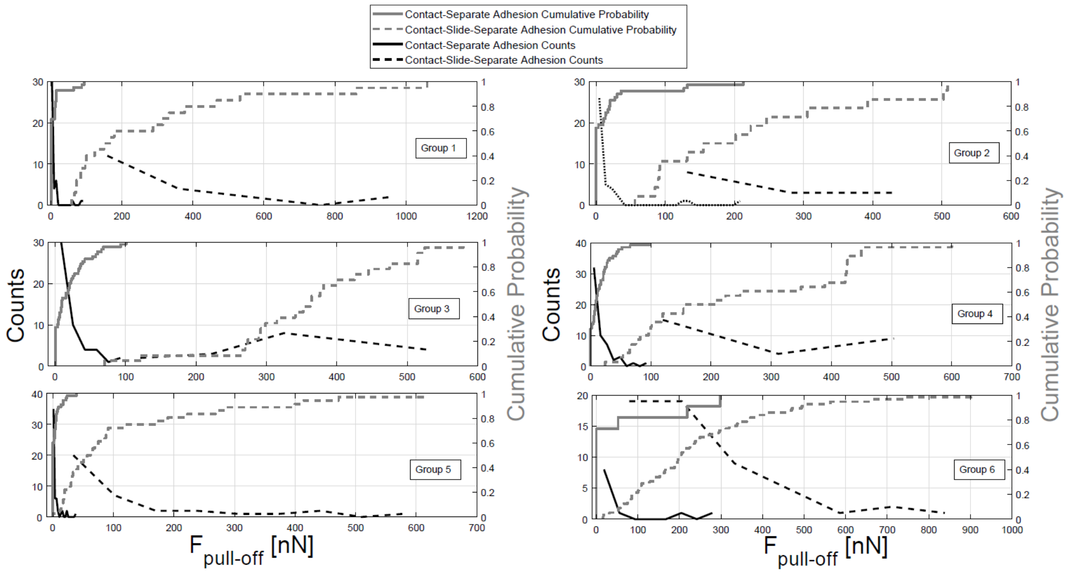

Figure 3 Statistics for the adhesion experiments. Shown are the cumulative probability of the pull-off forces (gray solid and dashed lines, right axes) versus pull-off forces and the counts (black solid and dashed lines, left axes) of the pull-off forces versus pull-off force, all demarcated by whether sliding was induced. The number of bins was calculated using the Freedman-Diaconis rule to more closely resemble the underlying distribution.

It was also observed that the rate of increase of adhesion with sliding speed was influenced by contact stress, which itself was estimated using the DMT contact mechanics approximation for normal stress of hard spheres with short-range adhesion. This dependence is shown in Figure 4 and grows quite linearly with the stress.

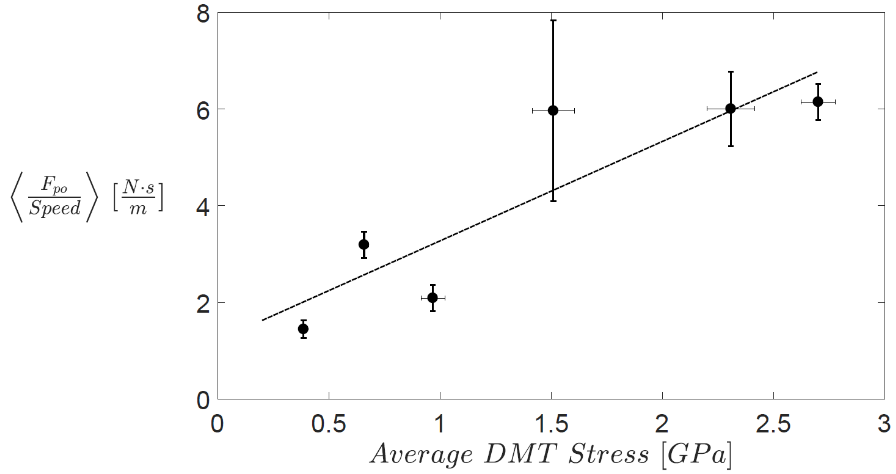

Figure 4 Average $\boxed{\frac{F_{pull-off}}{speed}}$ vs. average DMT stress for all contact-separate and contact-slide-separate tests. The dashed line is a linear fit. The error bars are standard deviations of the means.

We hypothesize that the reversible and stress-dependent nature of adhesion can be explained by the stress-modulated evolution of silicon surface passivation, as detailed in Figure 5. Initially, the silicon surfaces exposed to the TEM chamber after removing their oxide will be highly reactive and residual molecular hydrogen within the chamber will form silicon-monohydride bonds. These are low energy and thus highly unlikely to form bonds, which is why low adhesion is measured during CS tests. However, when sliding is induced, the high shear stress that arises from the speed dependence of friction vis-à-vis the thermal Prandtl-Tomlinson (PTT) model [3–7] will break the monohydride bonds and re-expose reactive silicon atoms, which can form covalent bonds across the interface, thus significantly increasing adhesion. Once the contact is separated, hydrogen repassivates the reactive surface, thus returning the surface to a low-energy state. The work of adhesion measured from CS tests was found to be $\boxed{8.7 \pm 13.6\frac{mJ}{m^2}}$, consistent with vdW interaction, while for CSS tests it was found to be $\boxed{145.5 \pm 92.7\frac{mJ}{m^2}}$ far greater than any previously reported values for any silicon termination and approaching the cleavage energy of Si(111).

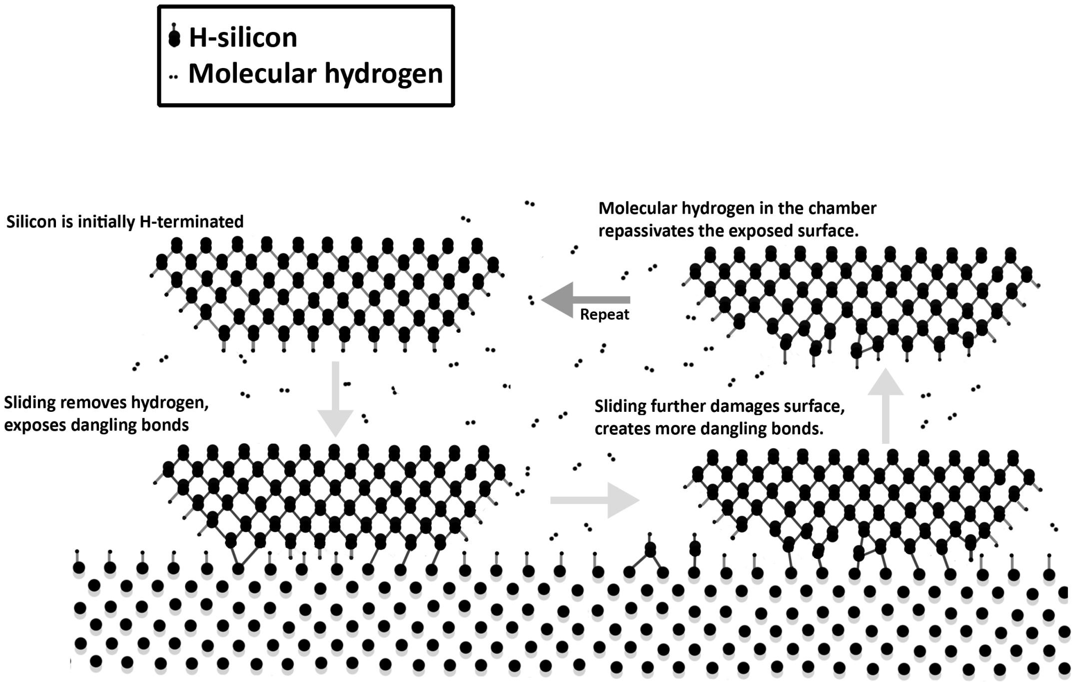

Figure 5 Illustration of the silicon-silicon adhesion mechanism.

A manuscript of this work has been submitted to Nature Materials (NM18072522) and is currently under review.

3.2 Silicon adhesion against diamond as a function of stress and speed

Diamond is the hardest known material and as such is an important surface to study in order to further develop applications where scratch and wear resistance is crucial such as hard-disk drive coatings and cutting tools. Diamond is also being looked at as a potential replacement for silicon in semiconductors and MEMS; diamond has a larger bandgap than silicon, is a better conductor of heat, and has superior electron mobility. Having a deeper understanding of diamond's surface properties and tribological mechanisms will be very useful for future commercialization. In this work, we performed *in situ* TEM nanoindentation of silicon nanoasperities sliding against flat diamond surfaces.

We found that adhesion of silicon sliding against diamond depends strongly on both contact stress and sliding speed. Molecular dynamics (MD) simulations performed by our collaborators of varying silicon probe roughness, diamond surface chemistry, and contact/sliding conditions complement the experimental studies. These coupled studies contribute to the growing body of adhesion research that is revealing the role of controlled energetic inputs such as temperature and normal and shear stress on interfacial chemical behavior.

3.2.1 Silicon asperities sliding against diamond show sliding-speed and stress-dependent adhesion

A fundamental mathematical description of the experimentally measured pull-off force of a spherical silicon tip on a flat diamond surface yields

$$\boxed{F_{eff} = F_{vdW} + F_{BOND} + F_{SUPP}} \qquad (1)$$

where $\boxed{F_{eff}}$ is the experimentally measured pull-off force. For a spherical tip against a flat surface, this effective force is a combination of several contributions. First is the van der Waals force of an ideal sphere against an ideal flat surface in the DMT approximation i.e., $\boxed{F_{vdW} = \frac{W_{vdW}}{2\pi R}}$, where $\boxed{W_{vdW}}$ is the van der Waals work of adhesion and $\boxed{R}$ is the radius of the sphere. Next is the force to cleave any bonds, $\boxed{F_{BOND}}$. Finally, any supplemental forces that arise either due to deviations from the ideal geometric assumptions arising from roughness can be condensed into one term, $\boxed{F_{SUPP}}$. Thus, the effective work of adhesion between a spherical tip and a surface can be defined as

$$\boxed{W_{eff} \equiv \frac{F_{eff}}{2\pi R} = W_{vdW} + \frac{F_{BOND}}{2\pi R} + \frac{F_{SUPP}}{2\pi R}} \qquad (2)$$

The effective work of adhesion for these tests $\boxed{W_{eff}}$, as defined in equation 2, is plotted against the normal contact stress in Figure 2. The normal contact stress $\boxed{\sigma_N}$, was calculated using the DMT model [18]. All tests were conducted at adhesion only i.e., with no external applied force.

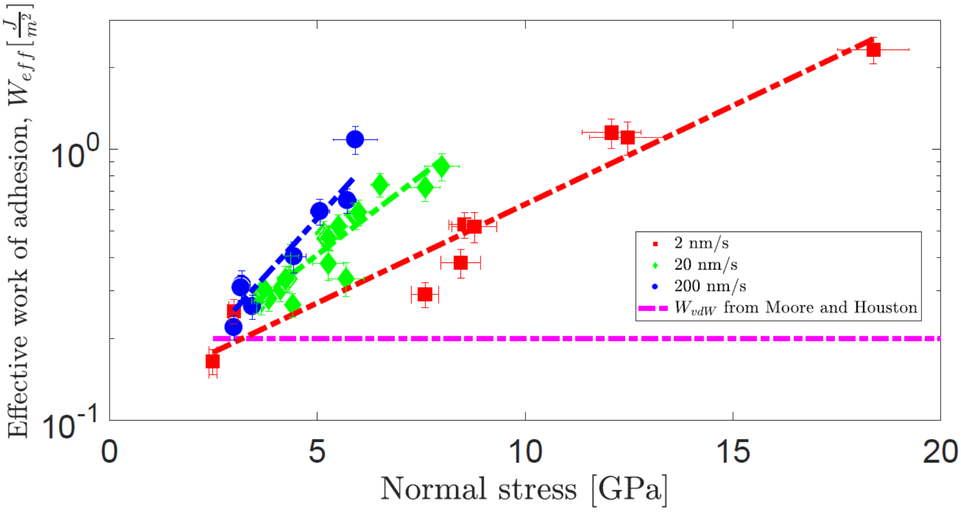

Figure 6 Effective work of adhesion plotted against the DMT normal contact stress for the speeds 2, 20, and 200 nm/s. The magenta line is an estimate of the ideal work of adhesion for silicon against diamond taken from Moore and Houston [8].

Remarkably, $\boxed{W_{eff}}$ increases exponentially with normal stress. $\boxed{W_{eff}}$ *also* increases with sliding speed for a given normal stress. Figure 7 illustrates the growth of exponential coefficient $\boxed{b}$ from a fit to the heuristic equation $\boxed{W_{eff} = a \exp\,(b \times \sigma_N)}$ on sliding speed, exhibiting the logarithmic trend.

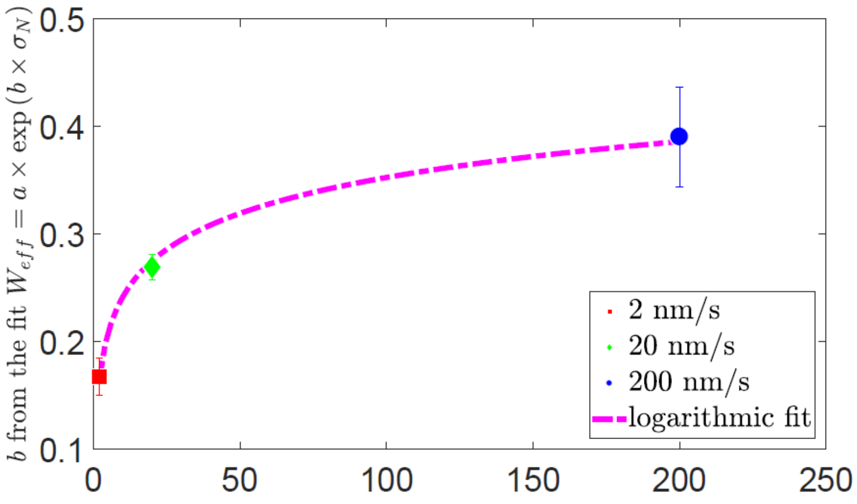

Figure 7 The slope from Figure 2 for each sliding speed, showing that the adhesion grows logarithmically with sliding speed

Simulations provide unique insights into the complex phenomena occurring in the interface between silicon and diamond. For this study, simulations with varying diamond hydrogen termination, applied force, silicon tip roughness, and sliding speed were performed. Figure 8 shows three time-sequential snapshots of a simulation of a rough silicon tip sliding on 100% Hydrogen-terminated diamond. It shows that the initially rough surface is smoothed out through plasticity and wear.

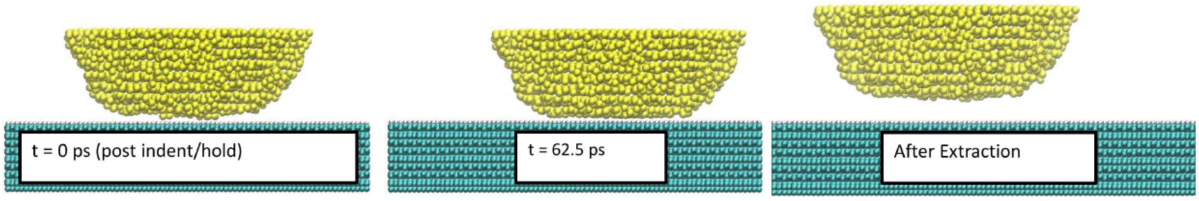

Figure 8 Sequential video snapshots from a simulation of a rough silicon asperity sliding against 100% H-terminated diamond. The roughness of the apex shown in the first frames is reduced during sliding and is apparent after contact is broken.

Relative to indent-only tests, the mechanism of smoothing during sliding tests increases adhesion. This is shown quantitatively in Figure 9 which displays force-distance curves for (a) indent-hold retract (IHR) tests and (b) indent-hold-slide-hold-retract (IHSHR) tests i.e., tests with sliding, for different applied forces. For IHR and IHSHR tests adhesion, which is the most negative normal force value, increases in magnitude when applied force increases. This is due to wearless and atomic-level plastic deformation due to irreversible compressing of protruding atomic asperities. Thus, we have identified one possible mechanism that modulates $\boxed{F_{SUPP}}$: stress and sliding-induced smoothing of the tip surface. This modulation likely only has an effect on the lower values of $\boxed{W_{eff}}$. Importantly, the true $\boxed{W_{adh}}$ i.e., $\boxed{W_{vdW}}$, must then lie somewhere between the lowest value reported in Figure 6 and the highest, with all changes of $\boxed{W_{eff}}$ smaller than $\boxed{W_{vdW}}$ with stress and speed occurring because of smoothing and changes in $\boxed{W_{eff}}$ larger than $\boxed{W_{vdW}}$ with stress and speed being dominated by stress-activated covalent bonding.

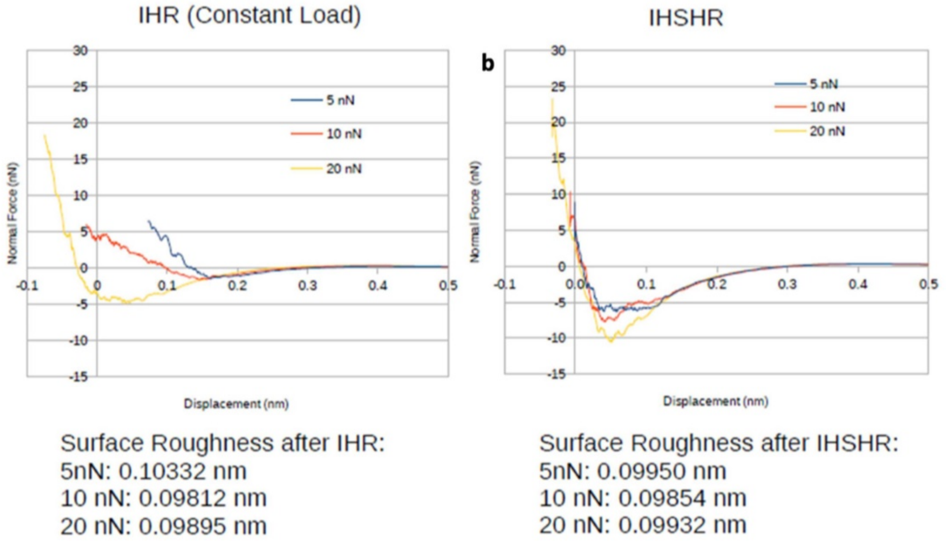

Surface Roughness after IHR:
5nN: 0.10332 nm
10 nN: 0.09812 nm
20 nN: 0.09895 nm

Surface Roughness after IHSHR:
5nN: 0.09950 nm
10 nN: 0.09854 nm
20 nN: 0.09932 nm

Figure 9 Force-displacement curves during retraction only for a rough silicon tip against 100% hydrogen terminated diamond from MD simulations for (a) indent-hold-retract and (b) indent-hold-slide-retract. Adhesion is greater in the case of sliding and also increases with increased applied force. Text below each graph indicates roughness values. Roughness does not change substantially from indenting or sliding.

A manuscript detailing this work is in preparation.

3.3 DLC wear and adhesion and the extended Multi Bond (eMB) wear model

Diamond-like carbon (DLC) has exceptional mechanical and tribological properties such as high hardness, low wear (in humid environments), and low friction. DLC is thus a material that is of great interest in several industrial and research applications such as hard disk drive coatings, cutting tool coatings, low friction surfaces, scanning-probe microscope coatings, and aerospace applications. For the latter application, it is necessary to properly quantify DLCs properties under a range of environmental conditions, but one very important environment is vacuum since space is a vacuum. Additionally, studies in vacuum eliminate the environmental variable such that results for a material pair are fundamental.

The wear and adhesion behavior of DLC asperities in vacuum has not been previously explored to the extent that silicon, another important material, has enjoyed. Nor has there been a concerted effort to compare wear behavior of DLC nanoasperities between environments. To fill in these gaps in knowledge we performed both *in situ* TEM wear and adhesion experiments in vacuum and *ex situ* AFM wear experiments in an environment with a small level humidity. To gain a better understanding of the adhesion results we collaborated with experts in molecular dynamics simulations at the United States Naval Academy and Oakland University. The wear results were analyzed with a new wear model developed in collaboration with researchers at Johns Hopkins University.

3.3.1 *ex situ* DLC AFM wear and extended Multi Bond (eMB) wear model

Seven DLC-coated AFM probes were worn at varying applied forces against Nioprobe surfaces in a controlled relative humidity of 3 ± 3%. The probes were imaged in TEM before wear, after specified intervals of wear against the Nioprobe surfaces, and after completion of the wear tests. Figure 10 shows TEM images of the seven probes used in this study before sliding, after 102 mm of sliding and after 512 mm of sliding. Progressive wear of the DLC coating is readily apparent and its severity correlates strongly with applied force, F_{ext}. Figure 11 shows AFM topography images from scans with the seven probes against Nioprobe surfaces. The gradual dulling of the probes is evident from the decreasing resolution of the sharp features of the Nioprobe surface as the experiments progress. Figure 12 displays traces of the two-dimensional TEM profiles of the seven DLC-coated probes imaged at specified intervals in the wear experiment.

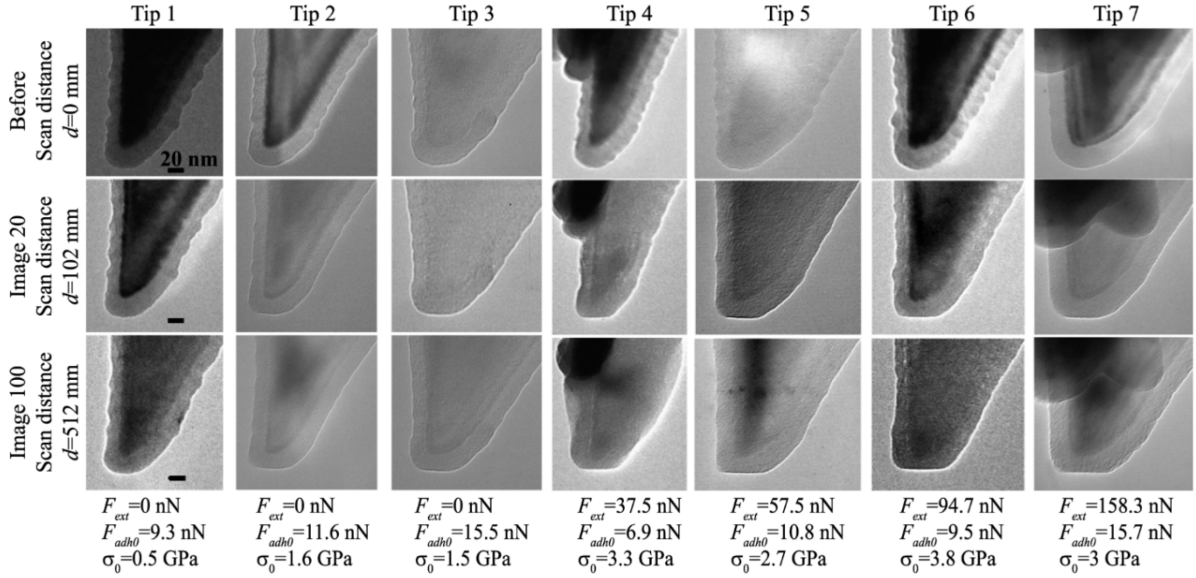

Figure 10 TEM images of the seven DLC-coated Si tips showing the evolution of tip geometry due to wear with sliding. Images of each tip before the wear scans (top row), after sliding for 102 mm (middle row), and after sliding for 512 mm (bottom row). The loading conditions, including the applied external load, F_{ext}, the initial adhesive load, F_{adh0}, and the calculated initial mean contact pressure, σ_0, are listed.

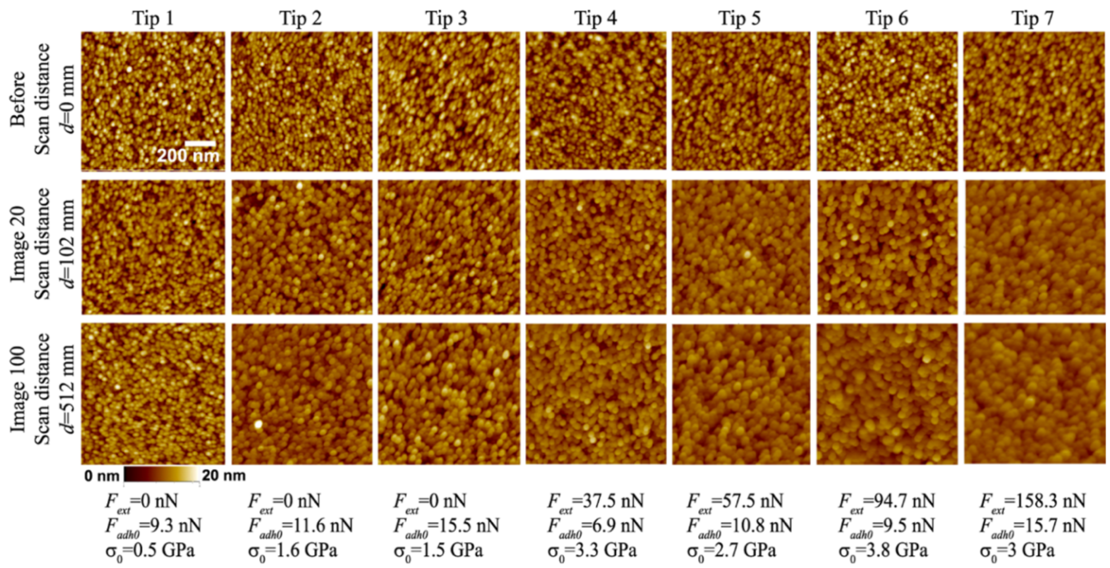

Figure 11 Contact mode topographic AFM images of Nioprobe surfaces acquired using tips 1−7 before the wear test (top row), after scanning 102 mm (middle row), and after scanning for 512 mm (bottom row). The in-plane (x−y) dimensions of the AFM images are 1 × 1 μm^2, and the z-height range of all AFM images is set at 20 nm (see contrast bar).

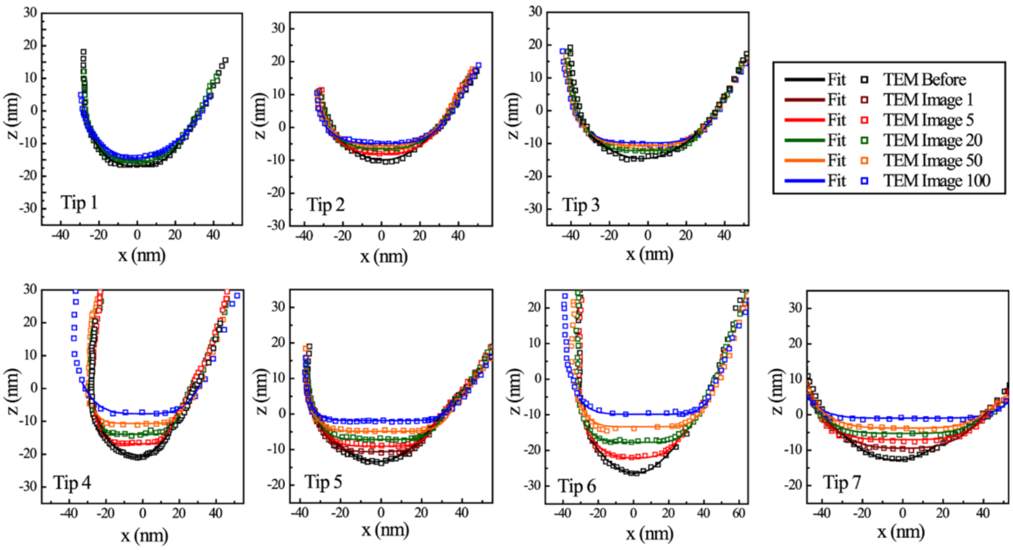

Figure 12 Two-dimensional (2-D) tip profiles extracted from the TEM images of tips at different scan distances. Symbols represent data obtained from image processing of TEM images, whereas solid lines are power-law fits to the tip profiles.

A recent model developed at the University of Pennsylvania describes a new wear process known as atom-by-atom (ABA) wear[1]. As the name suggests, ABA wear is gentle removal of single atoms, as opposed to the more commonly observed abrasive wear seen in macro and mesoscale studies. Using the wear volume obtained by subtracting probe volumes calculated from TEM images taken before and after sliding increments, $\boxed{V}$, along with DMT contact mechanics estimates of the contact area $\boxed{Area}$ (which uses the probe radius and total normal force), and also the sliding time, $\boxed{t}$, we estimated the reaction rate $\boxed{\Gamma_{\text{atom}-\text{loss}}}$ i.e., the rate at which atoms are lost due to wear, normalized by the average number of atoms in contact:

$$\boxed{\Gamma_{\text{atom}-\text{loss}} = \frac{V\times\rho_{volume}^{DLC}}{t\times Area\times\rho_{surface}^{DLC}}}. \qquad (3)$$

This equation relates directly to Arrhenius kinetics. An equation was proposed to compare the experimental data analyzed with equation 3 to a form consistent with Arrhenius chemical reaction rates i.e.,

$$\boxed{\Gamma_{\text{atom}-\text{loss}} = f_0 \exp\left(\frac{-\Delta U+\Delta V_{act}\sigma}{k_B T}\right)} \qquad (4)$$

where f_0 is the attempt frequency on the order of 10^{13} to 10^{14} s^{-1}, ΔU is the activation energy to wear an atom, ΔV_{act} is the activation volume, σ is the DMT normal stress, k_B is Boltzmann's constant, and T is the temperature. Figure 13 plots ABA wear results for all seven DLC probes using equation 3 against the DMT normal stress σ. Also plotted is a fit using equation 4, which shows good consistency with data at low stresses but is a poor fit at high stresses. To address this mismatch, a more general model of ABA wear was developed in conjunction with collaborators at Johns Hopkins University.

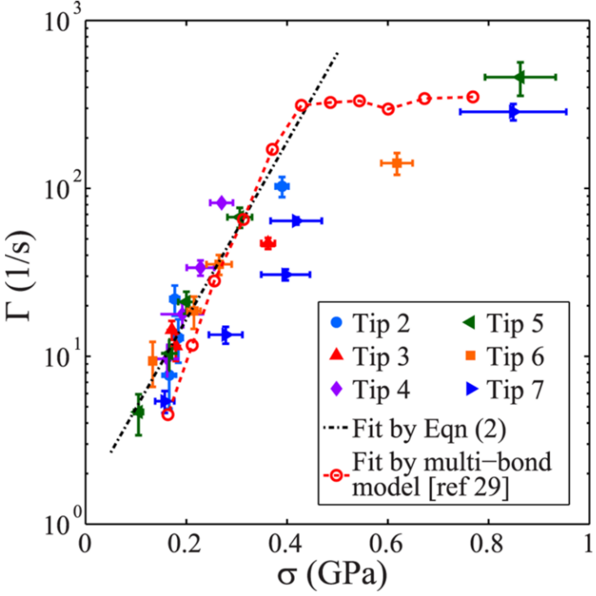

Figure 13 Normalized atomic wear rate (i.e., number of atoms removed from the tip per unit time normalized by the estimated number of atoms in contact) as a function of mean contact stress. Two models are fit to the data: (1) a transition state wear model is fit to data with σ < 0.3 GPa; and (2) a multibond model29 is fit to the full data set.

Figure 14 illustrates the more general kinetics model, which is dubbed the extended Multi Bond (eMB) model. Instead of the wear process being one-way i.e., a bond is formed then worn off, the possibility of the bond breaking without wear is included. In the terms used in Figure 14, an unbonded pair of atoms across the interface must first overcome the energy to bond, denoted as $\boldsymbol{\Delta E_{on}}$. In the low energy state of being bonded it can either wear off by overcoming the energy barrier $\boldsymbol{\Delta E_{wear}}$ (a.k.a. $\boldsymbol{\Delta U}$ from equation 4) or it can return to its original state by overcoming the energy barrier $\boldsymbol{\Delta E_{off}}$. All of these considerations lead to a more general statement of the reaction rate:

$$\Gamma_{\text{atom-loss}} = -\int_0^\infty \left(\frac{\Gamma_{wear}}{\Gamma_{off}+\Gamma_{wear}}\right)\left(\frac{\Gamma_{on}\times v}{(\Gamma_{off}+\Gamma_{wear}+\Gamma_{on})\times\Delta x}\right)\left(\frac{dP(\Delta x)}{d\Delta x}\right) d\Delta x \qquad (5).$$

Equation 5 is also plotted in Figure 13 illustrating the eMB model's ability to capture the ABA wear rate at an expanded range of stress where the cruder model of equation 4 cannot.

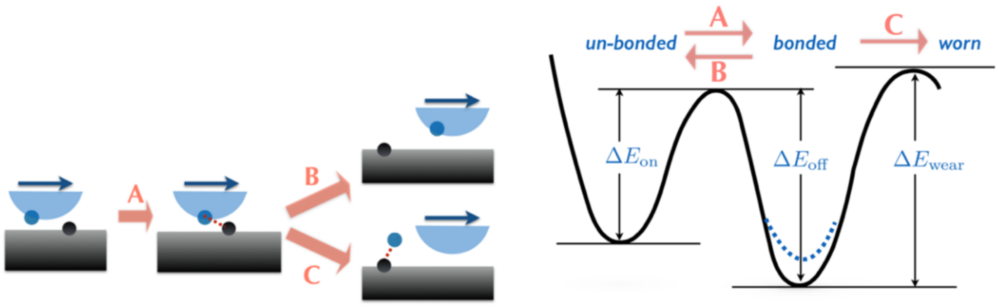

(a) (b)

Figure 14 A schematic of the multibond model with wear as an additional process. Transition A represents the formation of bonds between asperity and surface. B represents the breaking of these bonds while C represents the breaking of bonds in the asperity or surface. B represents the breaking of these bonds while C represents the breaking of bonds in the asperity or surface leading to wear.

Manuscripts detailing this work have been published [9,10].

3.3.2 *in situ* TEM DLC adhesion and wear coupled with molecular dynamics (MD) simulations

Using the *in situ* TEM nanoindentation tip on flat methodology, adhesion experiments of DLC probes on a flat diamond indenter were performed. Figure 15 illustrates this experimental setup. Five different tips were used to make and break contact many times in order to accumulate statistics for pull-in and pull-off forces and wear.

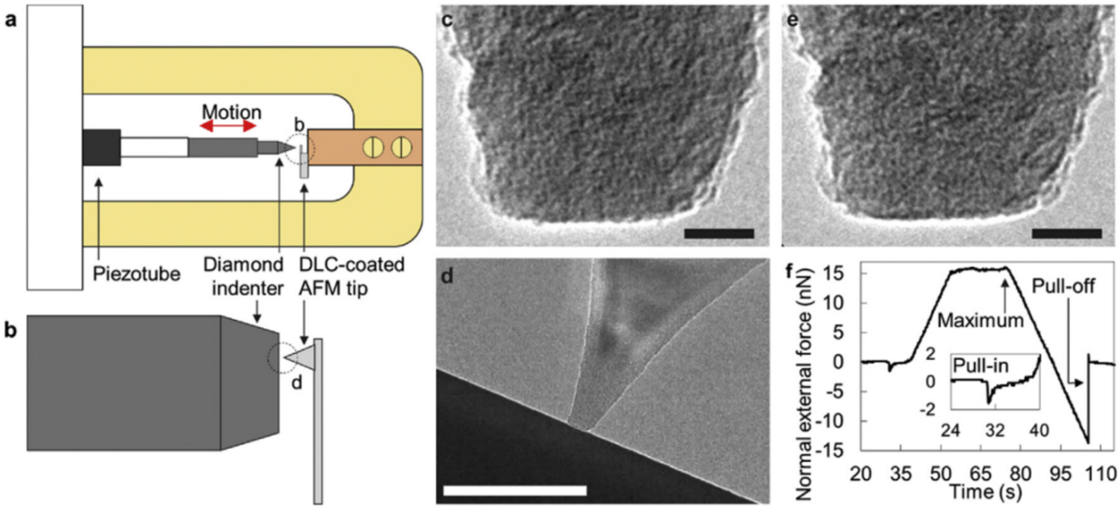

Figure 15 a. Schematic representation of the experimental setup using the Hysitron Picoindenter. The dashed circle is detailed in b, where a schematic close-up of the indenter and AFM cantilever is shown. c. Example of a high-resolution image taken before a contact (scale bar 10 nm). d. Frame of a video during contact (scale bar 200 nm). e. Example of a high- resolution image taken after a contact (scale bar 10 nm). f. Example of a time versus force curve extracted from the TEM videos, showing pull-in force, pull-off force and maximum external force. A close-up of the pull-in event is shown in the inset. d and f were obtained from the same contact event.

Figure 16 shows the evolution of pull-in and pull-off forces across a number of indents from one experiment as well as averages for all experiments. Clearly, the pull-off forces vary more than the pull-in forces. This occurs because pull-in forces are only affected by long-range attractions such as van der Waals (vdW) forces, which are a function only of the geometry, barring material differences. The variability in pull-off forces arises because of covalent interactions that form when in contact. The stochastic nature of bonding leads to large and random pull-off forces.

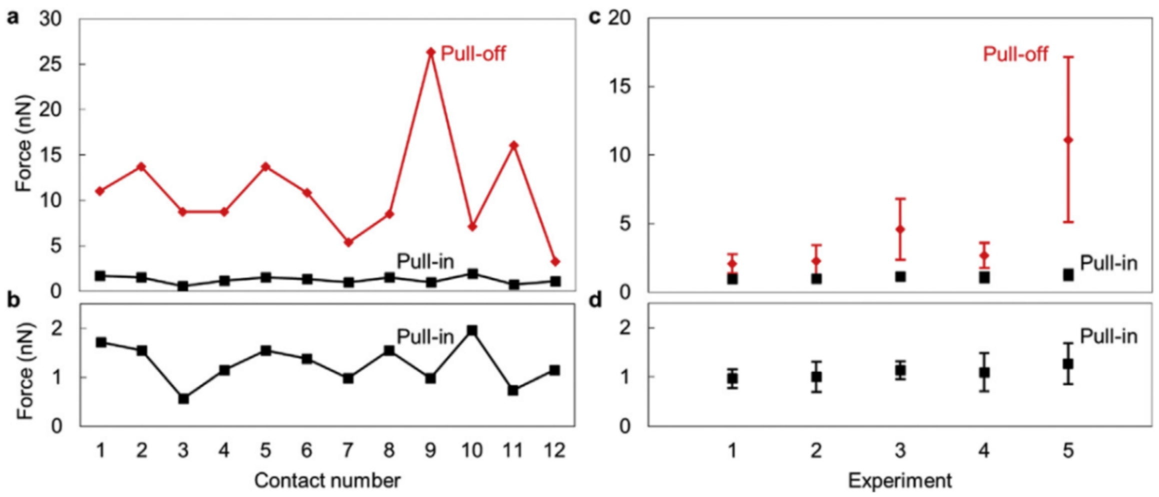

Figure 16 a. Evolution of the pull-in and pull-off forces as a function of consecutive contact number, for one of the experiments. b. Detail of the pull-in forces. c. Mean and standard deviation of pull-in and pull-off forces for all experiments. Experiment 5 corresponds to the data in a and b. d. Detail of the pull-in forces. (A color version of this figure can be viewed online.)

Simulations headed by collaborators at the United States Naval Academy and Oakland University provide further support for the covalent bonding hypothesis. Figure 17 illustrates both the simulated DLC probe and the diamond substrate (darkened areas on the substrate show the different regions where adhesion tests were performed).

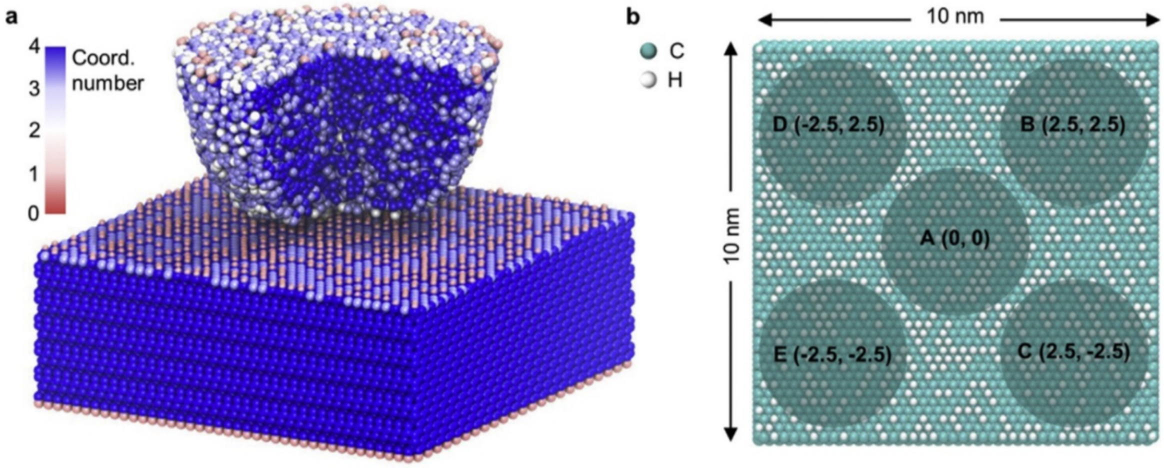

Figure 17 a. Perspective view of the MD simulation setup, with a cross section of the tip to see its internal structure. Small pink spheres represent hydrogen. Carbon atoms are colored by their coordination number. b. Top view of the H-terminated diamond (111) surface. Letters A-E represent different contact points of the tip.

Two different potentials were employed in this study, the AIREBO and the REBO-S. The AIREBO only simulates long-range forces such as vdW interactions and is therefore most appropriate for comparing to pull-in forces. Indeed, as Figure 18 **a** illustrates, pull-in forces (the lowest force in the Force-Distance plot) are very consistent despite the different regions they were measured in. Alternatively, the REBO-S potential models both long-range interactions and covalent interactions and is thus best suited for pull-off forces that are influenced by chemical bonds. As Figure 18 **b** shows, there is substantially more variability in pull-off forces between the different contact regions using the REBO-S potential; this is consistent with there being a stochastic nature to covalent bonding and consistent with what was observed experimentally.

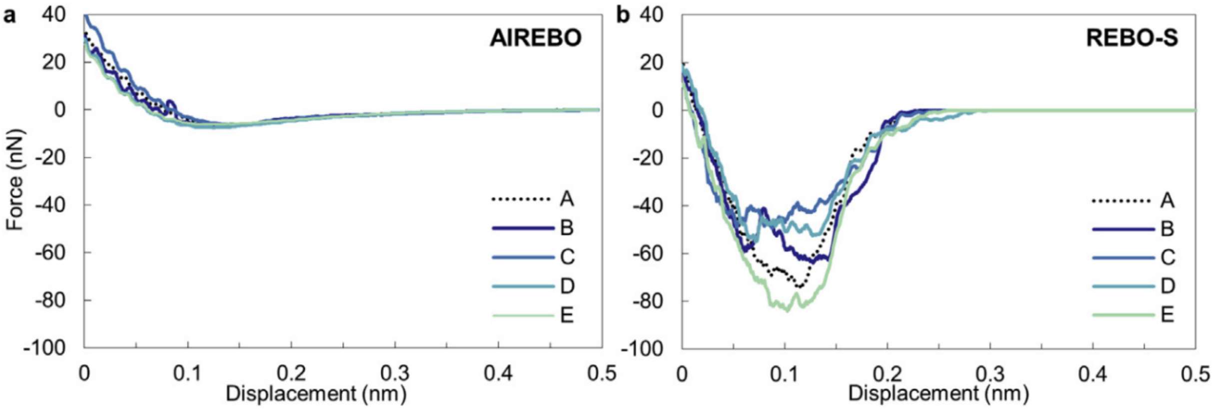

Figure 18 Simulated force versus displacement approach curves obtained using the a. AIREBO and the b. REBO-S potentials. Letters A-E correspond to different contact points on a 40% hydrogen terminated diamond surface.

This collaboration also produced the Hamaker constant of DLC in high vacuum 8.1 ± 9.7 x 10^{19} Joules. An Archard wear rate of 0.001 $mm^3/N.m$ was found consistently between experiments and simulations. This value is significantly higher than values reported for DLC in environment. The wear trends could not be fit by the ABA wear model of equation 4. Analysis is in progress to compare the wear results to the eMB model of equation 5 but it is quite possible that wear of DLC in vacuum (without a passivating environment) is too high to be explained by such a gentle wear regime. Finally, simulations produced results that were quite counterintuitive. Figure 19 shows that, for diamond surface hydrogen termination surface concentrations of 50% and less experience a smaller ratio of pull-off force to number of bonds when sliding is performed, suggesting that lower hydrogen terminations along with the induction of sliding lead to weaker interfacial interactions. This intriguing result is currently being studied closely in collaboration.

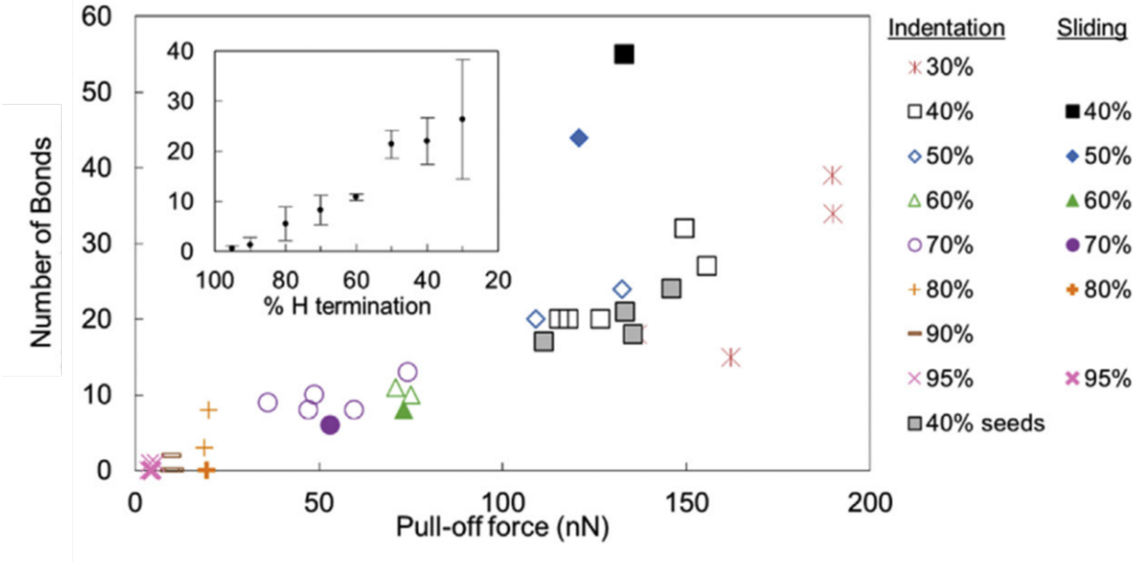

Figure 19 Effect of hydrogen termination on the pull-off force and number of bonds across the interface for both indentation and sliding. Inset summarizes the indentation results.

A manuscript detailing this work has been published [11].

3.4 Knowledge Transfer between the Collaborating Groups (Penn-CCU)

To strengthen collaboration between the two groups, since the last report, a graduate student from CCU, Yi Pan Lin, visited Prof. Carpick's lab and spent 2 weeks interacting with the postdoctoral researcher in Prof. Carpick's group, Dr. Rodrigo Bernal. This enabled the two groups to exchange information, methods, and knowledge, and to brainstorm on ideas. The student from CCU received extensive, hands-on training in the methods developed in Prof. Carpick's lab, and this enabled him to then to lead new experiments at CCU. Below are photographs from the visit.

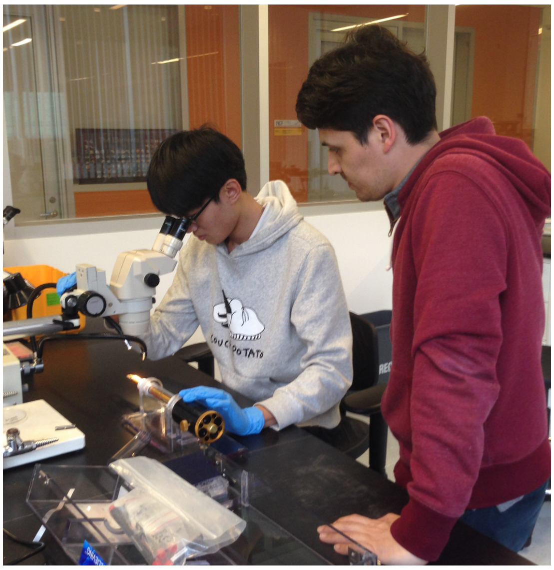

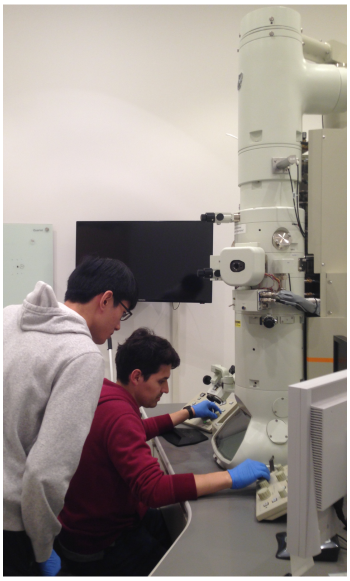

4 List of Publications and Significant Collaborations that resulted from AOARD support

4.1 Papers Published in Peer-Reviewed Journals

1. Bernal, R.A., Chen, P., Schall, J.D., Harrison, J.A., Jeng, Y.-R. and Carpick, R.W. *Influence of Chemical Bonding on the Variability of Diamond-Like Carbon Nanoscale Adhesion*. **Carbon** 128, 267-276 (2018). http://dx.doi.org/https://doi.org/10.1016/j.carbon.2017.11.040

2. Shao, Y., Jacobs, T.D.B., Jiang, Y., Turner, K.T., Carpick, R.W. and Falk, M.L. *Multibond Model of Single-Asperity Tribochemical Wear at the Nanoscale*. **ACS Appl. Mat. Interf.** 9, 35333-35340 (2017). http://dx.doi.org/10.1021/acsami.7b08023

3. Liu, J., Jiang, Y., Grierson, D.S., Sridharan, K., Shao, Y., Jacobs, T.D.B., Falk, M.L., Carpick, R.W. and Turner, K.T. *Tribochemical Wear of Diamond-Like Carbon-Coated Atomic Force Microscope Tips*. **ACS Appl. Mat. Interf.** 9, 35341-35348 (2017). http://dx.doi.org/10.1021/acsami.7b08026

4. Mangolini, F., Krick, B.A., Jacobs, T.D.B., Khanal, S.R., Streller, F., McClimon, J.B., Hilbert, J., Prasad, S.V., Scharf, T.W., Ohlhausen, J.A., Lukes, J.R., Sawyer, W.G. and Carpick, R.W. *Effect of Silicon and Oxygen Dopants on the Stability of Hydrogenated Amorphous Carbon under Harsh Environmental Conditions*. **Carbon** 130, 127-136 (2018). http://dx.doi.org/https://doi.org/10.1016/j.carbon.2017.12.096

4.2 Papers published in peer-reviewed conference proceedings

N/A

4.3 Papers Published in Non-Peer-Reviewed Journals or in Conference Proceedings

N/A

4.4 Conference Presentations without Papers

Invited

- **Opening Session Keynote Talk:** *Academic-Industry Partnerships in Nanotechnology: Stories from the Trenches*, TechConnect World 2017 Innovation Conference, Washington, D.C., May 2017.

- *Influence of Chemical Bonding on the Variability of Diamond-Like Carbon Nanoscale Adhesion: An In-Situ TEM/Nanoindentation and Molecular Dynamics Study*. Symposium on *In situ* Methods for Probing Properties and Dynamics in Materials, Microscopy & Microanalysis Conference (M&M) Baltimore, MD, Aug. 2018.

- *Nanotribology: A Route to Global Energy Efficiency Invited Speaker*. National Academy of Engineering Annual Meeting, Section 10 (Mechanical Engineering), Washington, DC, Oct. 2017.

- *Emerging Trends in Nanotribology, and their Implications for Manufacturing*. Manufacturing Science and Engineering Conference (MSEC 2017), Los Angeles, CA, Jun. 2017

- *An Examination of DLC Adhesion and Wear using MD and in-situ Nanoindentation*. STLE Annual Meeting, Atlanta, GA, May 2017.

- *Nanoscale Studies of Mechanisms of Tribological Behavior.* DENSO, Kariya, Japan. Feb. 2017.

Contributed

- *An Examination of the Nature of Bonding during Indentation and Sliding using MD and in-situ Nanoindentation*. Gordon Research Conference on Tribology, Lewiston, ME, July 2018.

- *Nanoscale Adhesion of Sliding Silicon Contacts is Increased by Speed and Stress*. STLE Annual Meeting, Minneapolis, MN, May 2018.

4.5 Manuscripts Submitted but not yet Published

Milne, Z.B., Bernal, R.A. and Carpick, R.W. *Sliding History-Dependent Adhesion of Nanoscale Silicon Contacts Revealed by in Situ Transmission Electron Microscopy*. **Nature Materials**. Under review. (2018).

5 Interactions with industry or with Air Force Research Laboratory scientists or significant collaborations that resulted from this work.

- AFRL collaboration. Started with A. Voevodin (formerly at AFRL, now at U. North Texas) and C. Muratore, continuing with N. Glavin and C. Muratore – U. Dayton/AFRL
- Industrial collaborations with Advanced Diamond Technologies Inc. (Gurnee, IL, USA), and Adama Innovations LLC (Ireland), on the development of diamond nanostructures for AFM probes.
- Collaborating with Hysitron Inc. (Minneapolis, MN, USA) on developing *in situ* tools.

6 References

1. Starr, M.J. and Segalman, D.J. *An Empirical Relationship for Extrapolating Sparse Experimental Lap Joint Data*. **J. Appl. Mech.-T. ASME** 78 (2011). http://dx.doi.org/10.1115/1.4003769
2. Segalman, D.J. *Modelling Joint Friction in Structural Dynamics*. **Struct. Control Hlth.** 13, 430-453 (2006). http://dx.doi.org/Doi 10.1002/Stc.119
3. de Boer, M.P. and Mayer, T.M. *Tribology of MEMS*. **MRS Bulletin** 26, 302-304 (2001).
4. Becker, E.P. *Trends in Tribological Materials and Engine Technology*. **Trib. Int.** 37, 569-575 (2004).
5. Tung, S.C. and McMillan, M.L. *Automotive Tribology Overview of Current Advances and Challenges for the Future*. **Trib. Int.** 37, 517-536 (2004).
6. Doll, G.L. and Evans, R.D. *Solving Wind Turbine Tribological Issues with Materials Science*. **Materials Science and Technology Conference and Exhibition 2010, MS and T'10** 3, 2158-2169 (2010).
7. Kotzalas, M.N. and Doll, G.L. *Tribological Advancements for Reliable Wind Turbine Performance*. **Phil. Trans. A** 368, 4829-50 (2010). http://dx.doi.org/10.1098/rsta.2010.0194
8. Grillo, S.E. and Field, J.E. *The Friction of Natural and CVD Diamond*. **Wear** 254, 945-9 (2003).
9. Konicek, A.R., Grierson, D.S., Gilbert, P.U.P.A., Sawyer, W.G., Sumant, A.V. and Carpick, R.W. *Origin of Ultralow Friction and Wear in Ultrananocrystalline Diamond*. **Phys. Rev. Lett.** 100, 235502/1-4 (2008). http://dx.doi.org/10.1103/PhysRevLett.100.235502
10. Erdemir, A. and Donnet, C., *Tribology of Diamond, Diamond-Like Carbon, and Related Films,* in

Modern Tribology Handbook, Vol. 2. (ed. B. Bhushan) 465-481 (CRC Press, Boca Raton, FL; 2001).

11. Chromik, R.R., Winfrey, A.L., Luning, J., Nemanich, R.J. and Wahl, K.J. *Run-in Behavior of Nanocrystalline Diamond Coatings Studied by in Situ Tribometry*. **Wear** 265, 477-89 (2008).
12. Hayward, I.P., Singer, I.L. and Seitzman, L.E. *Effect of Roughness on the Friction of Diamond on CVD Diamond Coatings*. **Wear** 157, 215-227 (1992).
13. Fontaine, J., Le Mogne, T., Loubet, J.L. and Belin, M. *Achieving Superlow Friction with Hydrogenated Amorphous Carbon: Some Key Requirements*. **Thin Solid Films** 482, 99-108 (2005). http://dx.doi.org/Doi 10.1016/J.Tsf.2004.11.126
14. Erdemir, A., Bindal, C., Fenske, G.R., Zuiker, C., Krauss, A.R. and Gruen, D.M. *Friction and Wear Properties of Smooth Diamond Films Grown in Fullerene + Argon Plasmas*. **Diam. Relat. Mater.** 5, 923-931 (1996).
15. Jeng, Y.R. *Impact of Plateaued Surfaces on Tribological Performance*. **Trib. Trans.** 39, 354-361 (1996). http://dx.doi.org/Doi 10.1080/10402009608983538
16. Jeng, Y.R., Kao, W.C. and Tsai, P.C. *Investigation into the Mechanical Contact Behavior of Single Asperities Using Static Atomistic Simulations*. **Appl. Phys. Lett.** 91 (2007). http://dx.doi.org/10.1063/1.2776019
17. Jeng, Y.R., Lin, Z.W. and Shyu, S.H. *Changes of Surface Topography During Running-in Process*. **J. Tribology** 126, 620-625 (2004). http://dx.doi.org/10.1115/1.1759344
18. Jeng, Y.R. and Peng, S.R. *Elastic-Plastic Contact Behavior Considering Asperity Interactions for Surfaces with Various Height Distributions*. **J. Tribology** 128, 245-251 (2006). http://dx.doi.org/10.1115/1.2162557
19. Jeng, Y.R. and Peng, S.R. *Atomic Simulation of Contact Behavior During Sliding Inception of an Asperity*. **Wear** 276, 70-74 (2012). http://dx.doi.org/10.1016/j.wear.2011.12.002
20. Kunze, T., Posselt, M., Gemming, S., Seifert, G., Konicek, A.R., Carpick, R.W., Pastewka, L. and Moseler, M. *Wear, Plasticity, and Rehybridization in Tetrahedral Amorphous Carbon*. **Tribol Lett** 53, 119-126 (2014). http://dx.doi.org/10.1007/s11249-013-0250-7
21. Konicek, A.R., Grierson, D.S., Sumant, A.V., Friedmann, T.A., Sullivan, J.P., Gilbert, P., Sawyer, W.G. and Carpick, R.W. *Influence of Surface Passivation on the Friction and Wear Behavior of Ultrananocrystalline Diamond and Tetrahedral Amorphous Carbon Thin Films*. **Physical Review B** 85 (2012). http://dx.doi.org/10.1103/PhysRevB.85.155448
22. Kim, H.I., Lince, J.R., Eryilmaz, O.L. and Erdemir, A. *Environmental Effects on the Friction of Hydrogenated DLC Films*. **Tribol. Lett.** 21, 53-8 (2006).
23. Jacobs, T.D.B. and Carpick, R.W. *Nanoscale Wear as a Stress-Assisted Chemical Reaction*. **Nat Nanotechnol** 8, 108-112 (2013). http://dx.doi.org/Doi 10.1038/Nnano.2012.255
24. Jacobs, T.D., Wabiszewski, G.E., Goodman, A.J. and Carpick, R.W. *Characterizing Nanoscale Scanning Probes Using Electron Microscopy: A Novel Fixture and a Practical Guide*. **Rev. Sci. Instrum.** 87, 013703 (2016). http://dx.doi.org/10.1063/1.4937810